Translational modeling of non-traumatic raised intracranial pressure in rodents; the impact of diet-induced obesity on cephalic hypersensitivity and retinal degeneration

Connar Stanley James Westgate[1]*, Snorre Malm Hagen[1,2]*, Ida Marchen Egerod Israelsen[1], Steffen Hamann[2], Rigmor Højland Jensen[1] and Sajedeh Eftekhari[1§]. *Contributed equally.

1. Danish Headache Center, Dept of Neurology, Glostrup Research Institute, Rigshospitalet-Glostrup, University of Copenhagen. Denmark. 2. Department of Ophthalmology, Rigshospitalet-Glostrup, University of Copenhagen. Denmark.

§Corresponding author: Sajedeh Eftekhari. Danish Headache Center, Department of Neurology, Glostrup Research Institute, Nordstjernevej 42, 2600 Glostrup, University of Copenhagen Denmark. Email: Sajedeh.eftekhari@regionh.dk

Westgate CSJ (connar.stanley.james.westgate@regionh.dk) Orcid ID 0000-0001-5066-8306

Hagen SM (snorre.malm.hagen@regionh.dk) Orcid ID 0000-0002-6644-8962

Israelsen IME (ida.marchen.egerod.israelsen@regionh.dk) Orcid ID 0000-0001-9765-0592

Hamann S (steffen.ellitsgaard.hamann@regionh.dk) Orcid ID 0000-0003-4318-2716

Jensen RH (Rigmor.jensen@regionh.dk) Orcid ID 0000-0001-6433-5887

Eftekhari S (Sajedeh.Eftekhari@regionh.dk) Orcid ID 0000-0002-5716-5725

Abstract

Elevated intracranial pressure (ICP) is a feature of critical cerebral disorders. Obesity has been linked to raised ICP, and especially to disorders such as idiopathic intracranial pressure (IIH). We aimed to explore the impact of diet-induced obesity (DIO) on ICP, cephalic sensitivity and structural retinal changes with the dual goal of developing a disease model for non-traumatic raised ICP and IIH. Rats were fed high-fat diet or matched control diet. To assess pain sensitivity, Von Frey and light/dark box testing were performed. Dual energy x-ray absorptiometry scanning was used to measure body composition. Optic nerve head and retinal structures were evaluated using optical coherence tomography. Intraocular pressure was assessed. Rats were then implanted with telemetric device for continuous ICP recording. At the end, eye histology and molecular analysis on choroid plexus (CP) and trigeminal ganglion (TG) were performed. The DIO rats had double the abdominal fat mass. ICP was 55% higher in obese rats (p=0.003). Altered pain thresholds were found in DIO rats as denoted by a lower periorbital threshold (p=0.0002). Expression of *Calca* and *Trpv1* was elevated in TG. Furthermore, a peripapillary retinal nerve fiber layer swelling (p=0.0026) with subsequent neuroretinal degeneration p=0.02) was detected in DIO rats. There was a trend to increased expression of AQP1 and NKCC1 at CP. This study demonstrates for the first time that DIO leads to raised ICP, with clinically relevant sequalae. Our novel model for non-traumatic raised ICP could expand the knowledge regarding disorders with elevated ICP and IIH.

Keywords: Obesity, intracranial pressure, idiopathic intracranial hypertension, retina, headache

Introduction

Elevated intracranial pressure (ICP) is observed in a range of cerebral pathologies, such as traumatic brain injury (TBI), ischemic stroke, hydrocephalus and idiopathic intracranial hypertension (IIH). These disorders are associated with significant morbidity and are amongst the most debilitating, costly brain disorders [1]. Currently, limited pharmacotherapies exist to treat patients with elevated ICP, as the mechanisms governing cerebrospinal fluid (CSF) production and ICP regulation and their dysregulation in pathology remain unresolved. The molecular pathway by which water crosses the choroid plexus (CP), the primary site of CSF secretion, is not fully characterized. However the characterization of aquaporin water channels (AQPs) and water co-transporting proteins such as the Na^+-K^+-$2Cl^-$-1 cotransporter (NKCC1) at CP have improved our understanding of this process [2]. Additionally, the effects of different physiological states on ICP and CSF secretion are poorly understood.

In recent years, studies have suggested that obesity is associated with ICP dynamics indicated by association between elevated BMI and ICP [3–5]. In support, a direct correlation between BMI, body fat percentage and CSF pressure has been demonstrated [5]. Furthermore, obesity is the major risk factor for development of IIH, which is a condition of increased ICP without identifiable cause. The condition affects mainly women and 90% of the patients are obese [6]. IIH has significant morbidity and the most common symptoms are chronic headache, cognitive impairment and impaired vision due to papilledema [7,8]. The severity of papilledema and visual loss in IIH is closely associated with increased BMI [9,10].

No proper preclinical model for non-traumatic raised ICP or IIH exists. The nature of IIH, with its atraumatic intracranial hypertension, chronic headache and impaired vision renders IIH an appealing model condition of elevated ICP that could provide valuable knowledge regarding both regulation and dysregulation of ICP pathophysiology. We previously demonstrated raised ICP in Zucker rats, a monogenetic genetic model of obesity [11]. However obesity is polygenic and the cause of IIH remain unelucidated, thus using a more physiologically relevant method of obesity is important for clinically applicability. In this study, we have therefore used DIO rats to explore the relationship between DIO, raised ICP, headache and the morphology of the optic nerve head and the retina. Our data reveals for the first time the impact of DIO on ICP with subsequent clinically relevant symptom development in the model.

Material and Methods

Animals and diets

64 female Sprague-Dawley (SD) rats (Taconic, Denmark) arriving at of 6 weeks (n=32) or 12 weeks (n=32) were used. At day of arrival rat were randomly allocated to either 60% high fat diet (HFD) (Research diets D12492) or matched control diet (CD) with 10% fat (Research Diets D12450J) for 15 weeks housed in the animal facility at Glostrup Research Institute, Denmark. Rats were left a week to acclimatize prior to all procedures. Food consumption and body weight were monitored weekly. Weight-based selection was made in the end of the diet for ICP implantation and eye examinations (Fig.1). The study was approved by the Institutional Animal Care and Use Committee, the Danish Animal Experiments Inspectorate (2014-15-0201-00256, 2019-15-0201-00365).

DEXA scanning

Body composition was estimated using a Lunar PIXImus DEXA scanner (GE Medical systems, Chicago). Scans were analyzed using LUNAR PIXImus 2 software in the region of interest generating values for lean mass (LM), fat mass (FM) and bone mass (BM). The region of interest was set to S1/L6 vertebral space to the L1/T12 vertebral space, thus scanning the abdomen [12].

ICP telemeter implantation and ICP recording

Selected animals from the DIO and control groups were implanted with ICP probes for continuous recordings (n=28), as previously described [13]. In brief, rats were anaesthetized with hypnorm/midazolam or ketamine/xylazine and the telemeter body was implanted in the abdominal cavity. The ICP catheter was tunneled under the skin to the parietal bone where the sensor tip was placed and secured epidurally. After surgery, the rats were placed in their home cages upon a Smartpad and ICP recording started. The telemeter sampled ICP at 2 kHz, where a Smartpad lowpass filter at 1

kHz gave a final sampling frequency of 1 kHz. After surgery and the two following days the rats received post-surgical treatments and were allowed to recover up to 7 days as described previously prior to co-housing [13]. On the postoperative days some of the rats lost weight (< 15%) and from day 7 weight increased as observed with this kind of procedure [13,14]. At the end of the experiments all animals were euthanized with an overdose of sodium pentobarbital. Few animals had to be sacrificed earlier due to adverse events such as opening of stiches and injection site reactions.

ICP analysis

ICP was measured for up to 30 days after implantation surgery. Presented means are for day of surgery, day 0 (n=9 CD, n=10 HFD), days 3, 7 and whole period (n=8 control, n=10 high fat). More specific spectral analysis of the ICP waveform was carried out on a 5-min stable section of ICP, i.e. without movement artefacts as previously described [13].

Measurement of hind paw and periorbital thresholds after mechanical stimulation

Von Frey testing was performed from diet start until day of surgery (day 0) (Fig.1). The sensitivity of the frontal region of the head (V1 ophthalmic trigeminal dermatome) and hind paw to static mechanical stimulation was measured using an electronic von Frey device fitted with a rigid plastic tip (IITC LifeScience Inc, USA). Testing was carried out as previously described [15]. The investigator was blinded to the experimental group during the experiment.

Light sensitivity

Photophobia was assessed by quantifying time spend in the light during a light/dark box test as previously described [16,17]. The light/dark box was placed in a dedicated room with video recording

where the rats were left to acclimatize before the test (HFD n= 24, CD n=24). Light intensity was set to 500 lux for 20 minutes. Time spend in the light (s) was assessed by blinded observers and defined as the eyes of the rats being visible in the light compartment of the box i.e. exposure to light. Photophobia was tested during their active period and for every round the rats were tested at the same day.

Optical coherence tomography and optic disk photography, image capture and analysis

Optical coherence tomography (OCT) and optic disk photography (ODP) of both eyes was performed prior to implantation of the ICP probe on day 0 (HFD n= 14, CD n=10, 48 eyes). OCT and ODP images were captured with a combined digital fundus microscope and image-guided spectral domain OCT system (Phoenix MICRON IV In Vivo Imaging Microscope and OCT2 system, Phoenix Technology). The corneal surface of eyes was topically anesthetized with Phenylephrine Hydrochloride 10% and pupils were dilated with Tropicamide 1%. The optic nerve head (ONH) was centered for the best OCT image. The OCT image was aligned horizontally, and optimized for best image quality through adjusting the polarization, contrast, gamma and dispersion. Peripapillary circular B-scans (1024 A-scans with a radius of 515 μm) were performed with 3-10 image averaging to reduce image noise. Finally, an ODP was captured with the optic disc centered and in focus.

From each eye, the best quality OCT images were analyzed using semi-automatic retinal segmentation software (InSight, Phoenix Technology). The inner limiting membrane (ILM), plexiform layer (IPL) and Bruch's membrane (BM) were automatically segmented and manually fitted for best accuracy, and additionally two layers (retinal nerve fiber layer (RNFL) and inner nuclear layer (INL)) were manually segmented. The thickness of the total retina (TR), the RNFL, the ganglion cell complex (GCC, which consists of the RNFL, the ganglion cell layer (GCL) and the IPL). All OCT segmentations and ODPs

were blinded for a neuro-ophthalmologist to evaluate. The ODP images were evaluated for obvious pathology including optic disc obscuration, peripapillary halo, vessel engorgement/torsion/obscurations, hemorrhages and choroidal folds. Intraocular pressure (IOP) was measured in non-anaesthetized rats on day 0 using a TONOLAB tonometer (ICARE, Finland). The investigator was blinded to both the experimental group and identity of the rat.

Histology of eyes

At the end of the study (day 30), eyes were collected and fixed in 4% paraformaldehyde in phosphate buffered saline (HFD n= 9, CD n=7, 32 eyes). The tissues were cryoprotected through immersion in raising concentrations of sucrose in Sörensen's phosphate buffer, followed by embedding in gelatin medium and cryosectioning at 12µm (Leica Microsystems GmbH). For morphological examinations, sections were stained by hematoxylin-eosin (HTX-Eosin). For measurement analysis, the best quality section from each animal covering the central portion of the ONH, and presenting the retinal nerve fibers entering the optic cup, were used for measuring the retinal nerve fiber bundle (RNFB) thickness at the level of the outer plexiform layer on each side of the ONH.

mRNA expression

CP and TG were removed from rats following sacrifice, immediately snap frozen and stored at -80°C prior to RNA extraction. Total RNA was extracted using Trizol reagent (Invitrogen^{TM}, Waltham, MA, USA). RNA was converted to cDNA using the Applied Biosystems High Capacity cDNA Reverse Transcription Kit (Life Technologies) according to manufactures instructions. qPCR was performed using the Applied Biosystems QuantStuio 6 Pro. Taqman Gene Expression Assays (Life Technologies) were used to assess gene expression. Reactions were carried out in 384 well plates, singleplex 10µl

reaction volumes, using Taqman Gene Expression Master Mix (Life Technologies) where samples were ran in triplicate. Genes expression was assessed using Taqman primer/probes sets, the genes assessed were *Aqp1* (Rn_00562834_m1), *Slc12a2* (Rn_00582505_m1), *Calca* (Rn_01511353_g1), *Ramp1* (Rn_01427056_m1), *Trpv1* (Rn_00583117_m1), *Tnf* (Rn_99999017_m1) and *Ilb1* (Rn_00580432_m1). Expression of the target genes was normalized to the expression of *Actb* (Rn_00667869) for TG and *Gapdh* (Rn_01775763) for CP. The relative expression of the gene is presented as fold change (2^-(ΔCt subjet)-(meanΔCt control)), statistics done on ΔCt values and arbitrary units.

Western Blot

Protein was obtained after extracting RNA from the samples with Trizol reagent (Invitrogen™, Waltham, MA, USA). Protein was extracted, precipitated and washed according to the manufactures protocol. The protein was solubilized in a solubilization with 1% sodium dodecyl sulfate. β-mercaptoethanol was added as a reducing agent making up 5% of the solution. Protein concentration was determined in triplicates on NanoDrop Spectrophotometer (NanoDrop™ 2000c, Thermo Scientific™, USA). The proteins were separated using 4-10 % bis-tris gel (Invitrogen™, USA) under gel electrophoresis and transferred to a polyvinylidene difluoride membrane (iBlot™, USA). The membrane was blocked, then incubated in primary antibody overnight diluted 1:1000 for Aqp1 (ab168387, Abcam), Lamin-B1 (ab65986, Abcam) and Nkcc1 (14581, Cell Signaling). Membranes were incubated in secondary antibody diluted 1:10000 and the protein bands were detected using chemiluminescent (Amersham™ ECL™, USA). The reaction was captured on luminescent image analyzer (LAS-4000 Luminescent Image Analyzer, Fujifilm, Japan). The resultant protein bands were

quantified using ImageJ (NIH, USA). The relative protein expression was normalized to the loading control (Lamin-B1) and presented as fold change from control.

Blood glucose

Blood glucose was measured on day 30, where the rats had been fasted overnight for at least 14h. Blood from the lateral tail veins was used to assess blood glucose (mmol/L) using glucometer ACCU-CHEK Aviva (Roche Diagnostics, Denmark).

Statistics

Statistical analysis was performed using Graphpad Prism 9 (Graphpad Software Inc, USA). Data presented as mean ± SEM or mean ± SD as stated. Data normality assessed via Shapiro-Wilk normality test. Where data was normally distributed unpaired two-tailed t-tests (equal variance) or Welch's test (unequal variance) was employed, whereas non-parametric data was assessed via Mann-Whitney U test. Pearson's correlation coefficient (r) was used for assessing correlations. Results were judged significant at $P<0.05$.

Results

Diet-induced obesity

Following obesogenisis, DIO rats selected for ICP surgery were 15.5% heavier (316±17.3 vs 365.9±37.8 g, P=0.002, table 1) with double the abdominal fat mass and 15% higher abdominal fat percentage (43.2±7.2 vs 28.9±3.2 %, P<0.0001, table 1) than selected controls. DIO rats included for ODP and OCT were heavier (370.8±35.5 vs 316.6±22.2 g, P=0.0002, table 1) with double the abdominal fat mass and 15% higher abdominal fat percentage (43.2±6.2 % vs 27.9±2.3, P<0.0001, table 1) than controls. No difference in fasting blood glucose between DIO rats and controls (6.3±0.49 vs 5.8±0.74 mmol/L, P=0.4) was detected.

DIO increases ICP

ICP telemeters were implanted in DIO and control rats in which ICP was continuously measured for 30 days. ICP was higher in DIO rats over the first 14 days (P=0.003, Fig 2A), where ICP on the day of surgery, day 0, correlated with abdominal fat percentage (r=0.54, P=0.016, Fig 2B). On day 0, DIO rats had raised ICP relative to control rats (2.77±0.57 mmHg vs -0.17±0.73, P=0.0052, Fig2 C, D). This raised ICP was associated with a right shift in ICP pressure frequency (Fig 2E). On day three, a day without the influence of post-surgical drugs, ICP was more than double in the DIO rats (4.6±0.74 mmHg vs1.46±0.06, P=0.0052, Fig 2F,G) also with a right shift in ICP (Fig 2I,H). Similarly, on day 7 when the rats have fully recovered from surgery [13], DIO rats had a higher ICP (5.17±0.47 vs 3.53±0.55 mmHg, P=0.03, Fig 2I,J) with a right shift in ICP (Fig 2K). From day 15 to 30 of recording there was no difference in ICP (P=0.2, Fig 2L). In the final 7 days recording, DIO rats had a trend to higher ICP than the control rats (5.94±0.55 vs 4.32±0.6 mmHg, P=0.07, Fig 2M). This loss of

significance in ICP could be mediated by weight loss. Although both groups lost weight as expected [13,14], DIO rats lost more weight before regaining weight to a lesser amount (-7.5±0.6% vs 0.6±1.7%, P=0.0004, Fig 2N).

To further analyze the ICP phenotype, ICP waveforms were assessed. On the day 0, there was no difference in any ICP frequencies, including those of slow non-respiratory ICP waves (0-0.25Hz) which are associated with pathological ICP features (0.29±0.07 vs 0.35±0.15 $mmHg^2$, P=0.4, Fig 3 A, B) However, we identified a 140% increase in spectral power of ICP wavelengths at 0-0.25Hz on day 3 (0.49±0.09 vs 0.20±0.08 $mmHg^2$, P=0.03, Fig 3C, D) and 350% increase on day 7 (1.09±0.3 vs 0.24±0.09$mmHg^2$, P=0.02, Fig 3E, F) after surgery.

DIO induces headache like behavior

All rats had cephalic and peripheral mechanical thresholds assessed during course of the diets. In the rats that started the diet at 12 weeks, the DIO rats had a lower threshold over the course of the diet (P=0.0038, Fig 4A), demonstrating cyclical periods of sensitivity. Rats that started the diet at age 6 weeks, showed no difference in threshold (P=0.4). This difference may be due to the challenges of getting the younger animals habituated to the test. The hind paw data showed that no difference over the course of the diet (P=0.4, Fig 4B).

On day 0 mechanical thresholds were assessed, where DIO rats were heavier (375.1±36.3 vs 313.8±22.7 g, P<0.0001) and had higher abdominal adiposity (table 1). DIO rats had lower periorbital (163.1±8.0 vs 213.8±5.1 g, P<0.0001, Fig 4C) and hindpaw (211.6±6.7 vs 237.0±6.1 g, P=0.01, Fig 4D) thresholds compared to controls, indicating prominent cephalic and modest peripheral mechanical cutaneous allodynia in DIO rats. Periorbital thresholds show a strong inverse correlation with

abdominal fat percentage (r=-0.65, P=0.0005, Fig 4E). ICP was not correlated with cephalic withdrawal thresholds on day 0 (r=-0.236, P=0.4). We assessed light sensitivity as a measure of photophobia. The control and DIO rats spend equal time in the light during the test (22.8 % ± 2.5 vs 24.3 % ± 2.4., P=0.69, Fig 4G).

To further interrogate the headache phenotype, we assessed gene expression in TG on day 30 (Fig 4F). In the DIO rats, there was a 1.25 fold increase in *Calca* (CGRPα) expression (2.9±0.05 vs 3.41±0.15 ΔCt, P=0.002) and a 1.29 fold increase in *Trpv1* expression (5.94±0.0.06 vs 6.35±0.14 ΔCt, P=0.018) compared to controls. No differences in expression of *Ramp1* (P=0.58) or the pro-inflammatory genes *Tnf* (P=0.78) and *Il1b* (P=0.70) were found.

Retinal swelling and degeneration in DIO

The ODPs in both groups appeared normal without any notable pathology or any signs of acute papilledema (Fig. 5). The OCT scans showed no significant thickness difference between right and left eye in any of the retinal layers (Table 2). No difference in thickness between DIO and control animals was found for TR, GCC, IRL and ORL (Fig. 5C). The RNFL was thicker in the DIO (28.81±0.61 vs 24.85±1.093 µm, P=0.0026, Fig. 5D) compared to control animals and thus swollen. RNFL thickness was associated with ICP (r=0.639, P=0.0058, Fig. 5E), weight (r=0.56, P=0.0048, Fig. 5F) and DEXA abdominal fat percentage (r=0.469, P=0.02, Fig. 5G). No significant difference in IOP was found (15.73±0.872 vs.13.72±0.760, P=0.102).

To investigate the anatomical consequences of raised ICP at the RNFL, the thickness of the retinal nerve fiber bundle (RNFB), a structure comprising of RNFL axons, was assessed. DIO animals had

thinner RNFBs (74.372±3.624 vs 88.364±3.974 µm, P=0.0214, Fig. 5I) compared to control animals, indicating RNFB degeneration.

Expression at CP

In CP, mRNA expression of *Nkcc1* in the DIO rats displayed a 1.16-fold change (821±118 vs707±71, AU, P=0.43, Fig.6A) and by 1.66-fold change of *Aqp1* (41±10 vs 33±7, AU, P=0.56, Fig.6A). The same trend was also observed by immunoblotting. The protein expression of Nkcc1 showed a 1.3-fold (4.7±0.92 vs 3.4±0.78 AU, p=0.43,Fig.6C).Total Aqp1 was displayed a 2.2-fold change (5.3±1.5 vs 2.4±0.5, AU, P=0.1,Fig.6D), where by the ratio of glycosylated Aqp1 to total expression showed a 1.3-fold (0.59±0.06 vs 0.46±0.03 AU, P=0.084, Fig.6E).

Discussion

In the current study we have investigated the impact of DIO on ICP and developed the first animal model for non-traumatic raised ICP demonstrating relevant sequalae mimicking the clinical IIH phenotype. Here we show that DIO rats develop raised ICP, headache related hypersensitivity and neuroretinal degeneration. This is critical, as recent data strongly suggests that obesity causes elevated ICP [3,11,18,19]. This is important considering the obesity pandemic, where the therapeutic approaches to management of elevated ICP are virtually absent and molecular mechanisms causing raised ICP remain unidentified. Our new animal model may change this.

Impact of obesity on ICP and CP alterations

A recent study demonstrated that in a mixed neurological patient cohort, BMI and percentage body fat both positively correlated with CSF opening pressure, although to a lesser degree than seen in IIH patients [5,20]. Here we demonstrate raised ICP in the DIO group, where the ICP was raised by 55% in the DIO rats, which associated with increased abdominal obesity in agreement with the clinical literature [5]. This study is congruent with our previous study where genetic obesity in rats caused 40% higher ICP [11]. We have recently shown that with normal weight gain in rats, there was a trend to an increase in ICP, supporting the concept of adiposity impacting ICP [13]. This data thus confirms excess adiposity alters CSF dynamics. Indeed previous data suggests that obesity increases CSF secretion in obese female rats without alterations in CSF drainage [21]. In agreement with this we demonstrate increased spectral power of non-respiratory slow waves after surgical recovery in DIO rats. This potentially indicates altered cerebral compliance and therefore cerebral pathology as seen in several human ICP disorders [22].

These data and those of others indicate that obesity has a direct effect on ICP, however no adipose derived factors have been explicitly demonstrated to raise ICP. However, glucocorticoids (GCs), hormones known to be increased tissue level activity in obesity, have been demonstrated to increase CSF secretion without altering CSF drainage suggesting that GC have the capacity to alter CSF dynamics [21,23]. Whether the observed increase in ICP in the obese animals is due to obesity, endocrine abnormalities or other neurochemical disturbances caused by obesity is yet unknown. Future investigations into obesity specific factors will help elucidate the molecular underpinnings of DIO mediated raised ICP. A technical limitation of the current study is not performing ICP recording during obesogenesis, thus preventing the observation of the temporal development of raised ICP. Although the use of female rats makes this work relevant to IIH, further studies assessing the effect of DIO on male rats will help complete our understanding.

In the current non-traumatic raised ICP model, there was only a trend to increased mRNA expression of *Aqp1* and *Slc12a2* at CP. This trend was also observed in protein expression, where there was tendency to increased ratio of glycosylated AQP1 to total AQP1. This is in contrast to our previous results where Zucker rats with elevated ICP had increased expression of AQP1 at CP [11]. This can be accounted for due to slower post-surgical weight gain in the DIO rats. The weight difference at 30 days was decreased to 3,4%. This may have affected the outcome in the molecular analysis and therefore requires further investigation. All together this suggests that the obesity-induced raised ICP may modulate CSF dynamics by altering the expression of the water channels but further studies are warranted here.

Obesity, raised ICP and headache development

Headache is associated in pathologies with raised ICP such as TBI, hydrocephalus and IIH [24]. Thus, headache is the key symptom in 75-94% of IIH patients at diagnosis[25–27]. In the present study, we show that DIO rats had cephalic cutaneous mechanical allodynia but not peripheral in the context of raised ICP, where the severity was closely associated with higher levels of abdominal obesity. The altered pain thresholds were cyclical after 5 weeks on the diet. Cephalic cutaneous allodynia is considered to be a measurement of central sensitization to pain and a marker of progression to migraine chronification in humans[28]. The present study adds novel data to the few experimental studies suggesting that obesity increases headache like behavior in rodents, where DIO increased facial pain behavior, and in contrast to our data, photophobic behavior in mice [29,30]. We did not find any difference in the light sensitivity between the DIO and control animals suggesting that these animals are not photophobic. Such difference could be accounted for different species between studies or use of fewer animals. Importantly, our data mirrors the human data, where obesity is associated with increased incidence of headache, where increased abdominal obesity confers both an increased risk of migraine diagnosis and increases cutaneous allodynia severity [28,31]. No link between ICP and cephalic thresholds was found, mimicking the clinical features of IIH, where ICP did not correlate with the reported headache severity [25]. In support of this, the vast majority of patients with IIH continue to experience disabling headaches after the other manifestations of the disorder including raised ICP has resolved [25].

In agreement with our behavioral data, we demonstrate increased expression of trigeminal ganglion *Calca* and *Trpv1* in DIO rats. It is clear that CGRP plays a key role in headache disorders and inhibition of CGRP signaling has demonstrated clinical efficacy as migraine therapy [32]. Furthermore,

increasing attention has been given to the capsaicin-gated channel, transient receptor potential vanilloid subfamily member 1 (TRPV1), suggested to play a role in migraine and related sensitization [33]. Thus, the increased expression of these genes suggests increased molecular sensitivity of the TG to nociceptive stimuli. This cutaneous allodynia was present in the absence upregulated pro-inflammatory genes. The direct cause of the molecular alterations and therefore cutaneous allodynia remains uncertain. The raised ICP through direct mechanical stimulation of the dura mater and TG, through raised ICP, could increase sensitivity. Additionally, obesity related factors could be involved. Further work to elucidate the underpinnings of the cutaneous allodynia is required.

Neuroretinal changes

Raised ICP is known to cause papilledema and visual decline. In this study, the OCT data showed thickening of the peripapillary RNFL in DIO rats with a positive correlation to ICP, suggesting axonal swelling. Across both the DIO and the control animals, there was also a clear correlation between RNFL thickness and the total body weight and the abdominal fat percentage. This indicates abdominal obesity is a potential disease aggravating factor. Moreover, this highlights that ICP is likely involved in the retinal phenotype present in this experimental model. Histological analysis demonstrates that after a prolonged period of DIO and elevated ICP there was a significant thinning of RNFBs entering the optic disc. This is in accordance with clinical findings, where obesity is found to correlate with both raised ICP and RNFL thinning [34,35]. To our knowledge this is the first animal model to demonstrate a link between obesity induced ICP elevation and retinal nerve fiber degeneration. The link between ICP and neuroretinal degeneration has previously been demonstrated in mouse models of sustained and robust elevated ICP which caused papilledema with neuroretinal and optic nerve degeneration [36,37]. No signs of acute papilledema were detected in the present study, which may be explained by the mild ICP

increase that occurs in this non-traumatic model. Even in a rat hydrocephalus with markedly increased ICP (> 15 mmHg) only modest signs of acute papilledema were detected. The mechanisms underlying the RNFL swelling and subsequent degeneration remain unclear, future studies to determine if the observed phenomena are a consequence raised ICP or another obesity related process is required. The presence of similar fasting glucose and IOP levels suggest that diabetic retinopathy and glaucomatous optic neuropathy are not influencing factors in this model.

Conclusions

This study demonstrates for the first time the neuroophthalmological manifestations of DIO with raised ICP and the clinically relevant sequalae of headache like behavior and retinal degeneration in rodents. These findings contribute to the understanding of the impact of obesity on brain health and the neurobiology of raised ICP disorders, especially IIH. This non-traumatic raised ICP model provides tools that can be utilized in the future evaluation of underlying molecular mechanisms and the development of novel ICP reducing agents to determine their efficacy.

List of abbreviations: AQP1=aquaporin 1, CD=control diet, CGRP=calcitonin gene related peptide, CP=choroid plexus, CSF=cerebrospinal fluid, DIO=Diet induced obesity, FM=fat mass, GC=glucocorticoids, HFD=high fat diet, ICP=Intracranial pressure, IIH=Idiopathic intracranial hypertension, IOP=Intraocular pressure, LM=lean mass, mmHg=millimeters of mercury, NKCC1=Na^+-K^+-$2Cl^-$-1 cotransporter, OCT=optical coherence tomography, RNFB=retinal nerve fiber bundle, RNFL=rentinal nerve fiber layer, TBI=traumatic brain injury, TG=trigeminal ganglion, TRPV1=transient receptor potential vanilloid subfamily member 1.

Declarations

Ethics approval: The study was approved by the Institutional Animal Care and Use Committee, the Danish Animal Experiments Inspectorate (2014-15-0201-00256, 2019-15-0201-00365).

Consent for publication: Not applicable

Availability of data and material: The datasets used and/or analysed during the current study available from the corresponding author on reasonable request

Conflict of interest: The authors declare that they have no competing interests

Funding

The Candys Foundation, Lundbeck foundation (grant nr 276), A.P. Møller Foundation and International Headache Society fellowship grant.

Author Contributions

Westgate CSJ, Hagen SM and Israelsen IME performed experiments, analyzed data, and contributed to writing of the manuscript. Hamann S analyzed eye data and contributed to writing of the manuscript. Jensen RH designed the study and contributed in the writing of manuscript. Eftekhari S designed the study and the experiments, performed experiments, analyzed data, and wrote the manuscript. All authors reviewed and approved the final version of the manuscript.

Acknowledgements

Professor Niklas Rye Jørgensen and PhD Maria Ellegaard Larsen at Glostrup Research Institute for the use of the DEXA scanner.

Professor Birgitte Holst, Professor Nanna MacAulay and assistant professor Jonathan Wardman at Copenhagen University for valuable discussions.

Thank you to David Møbjerg Boslev Kristensen at Glostrup Research Institute for his critical reading of the manuscript.

Figures and tables:

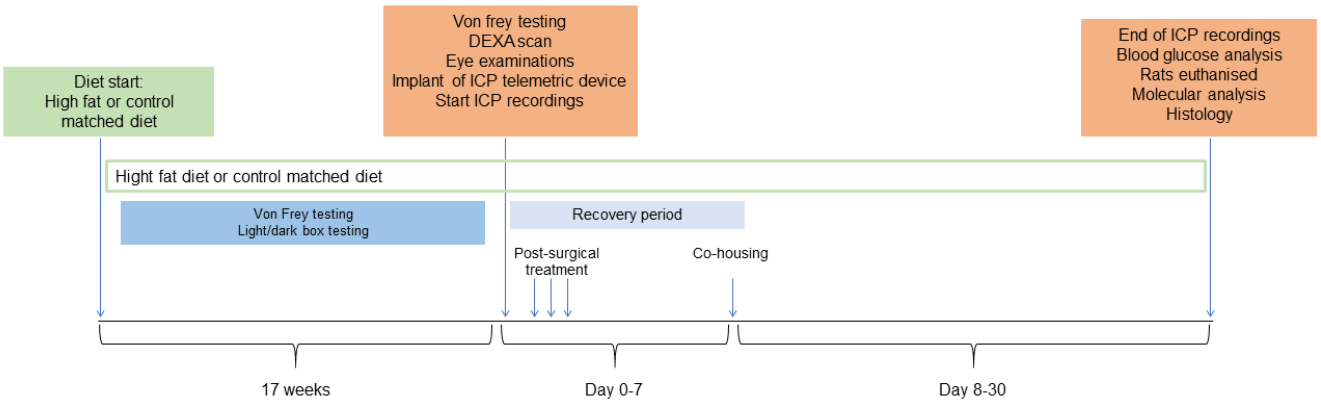

Figure 1. Study design: Experimental design. Female rats were on high fat diet or control matched diet for 17 weeks. Von Frey testing was performed during the whole diet period. Following the 17 weeks, Von Frey testing, DEXA scanning and all the eye examinations were performed followed by implantation with ICP telemetric probe for continuous ICP recording (day 0). During the recovery period (day 0-8), the rats were kept single-housed to recover from the surgery and then co-housed (from approximately day 8). Day 8-30 the rats were not affected by anesthesia or any drugs and ICP recordings was continued until day 30.

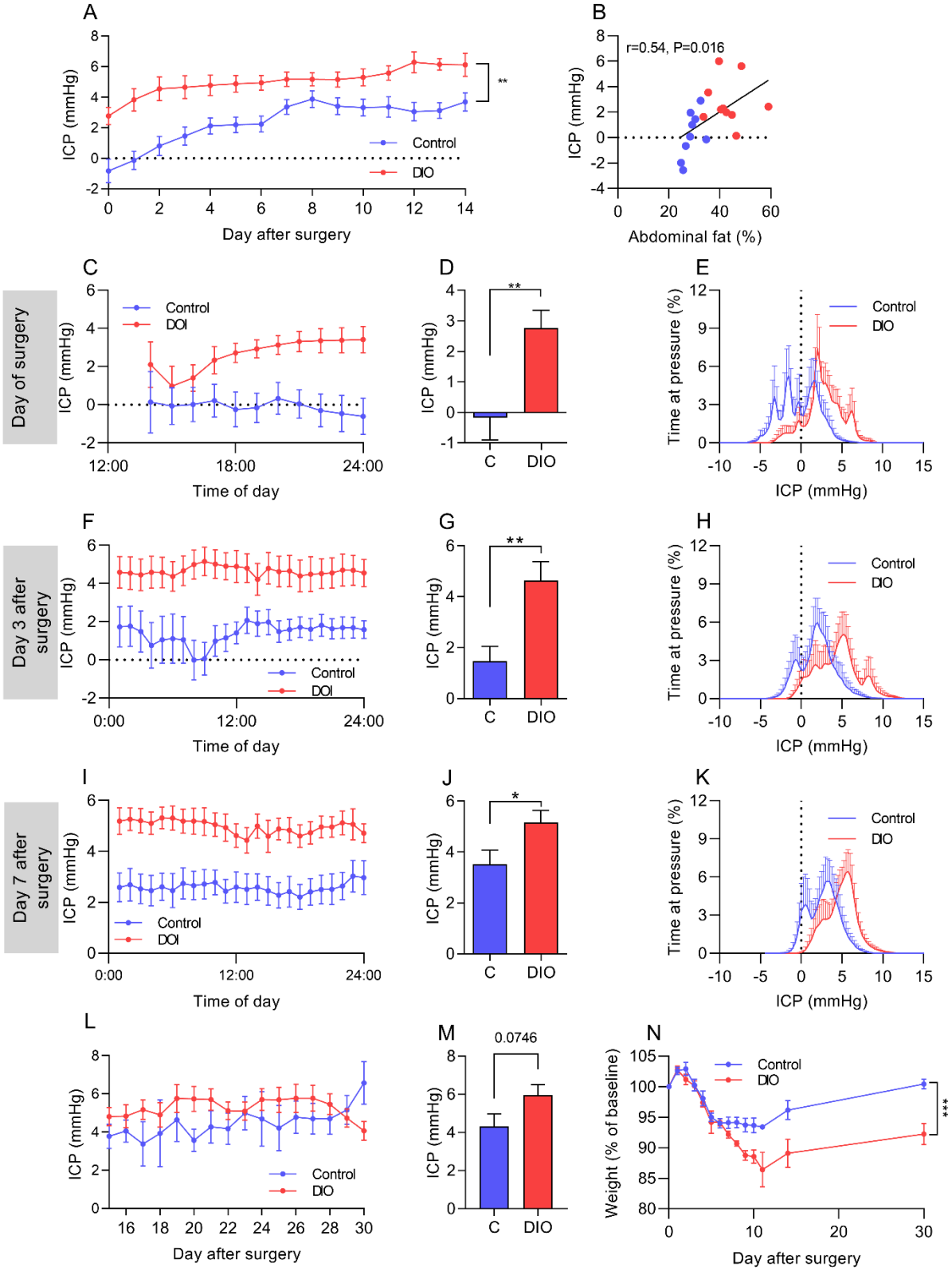

Figure 2. DIO increases ICP in female rats: Female Sprague-Dawley rats on control and very high fat diet implanted with ICP probes for 30 days. (**A**) ICP pressure trace over the 14 day ICP monitoring period. (**B**) Scatter graph depicting abdominal fat % vs ICP on day 0. (**C**) ICP pressure trace on day 0. (**D**) Mean ICP on the day of surgery. (**E**) Pressure frequency on day of surgery (**F**) ICP pressure trace on day 3. (**G**) Mean ICP on day 3. (**H**) Pressure frequency on day 3 (**I**) ICP pressure trace on day 7. (**J**) Mean ICP on day 7. (**K**) Pressure frequency on day 7. (**L**) ICP trace from day 15 to 30, note that multiple data points are missing. (**M**) Mean ICP over the final 7 days of ICP recording. (**N**) Weight loss and regain following surgery. Control N=9, DIO N=10. Two-way repeated measures ANOVA for A,L and N. Pearson's correlation for B and unpaired students T-tests for D, G, J and M. *=$P<0.05$, **=$P<0.01$. Data presented as mean±SEM.

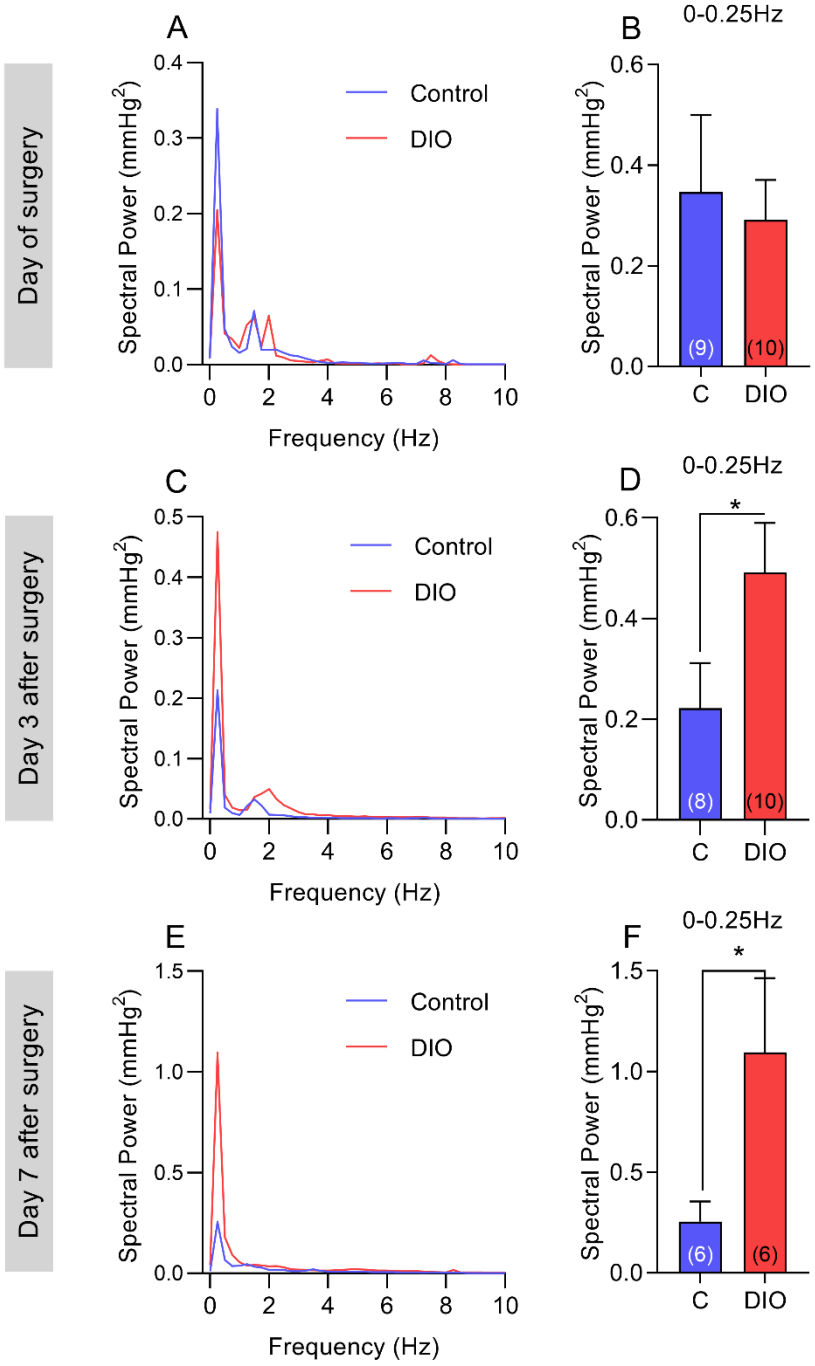

Figure 3. DIO alters ICP waveforms: Fast-Fourier transformation analysis of ICP waveforms between control and DIO rats. Power spectrum of ICP on day 0 (**A**) 3 days after surgery (**C**) and 7 days

after surgery (**E**), condensed into 0.25Hz bins. Spectral power of slow ICP waves on day 0 (**B**), 3 days after surgery (**D**) and 7 days after surgery (**F**). N for each time point can be found in parentheses in the figure. Unpaired T-tests for B,D and F. *=P<0.05. Data presented as mean for A,C and E, mean±SD for B,D and F.

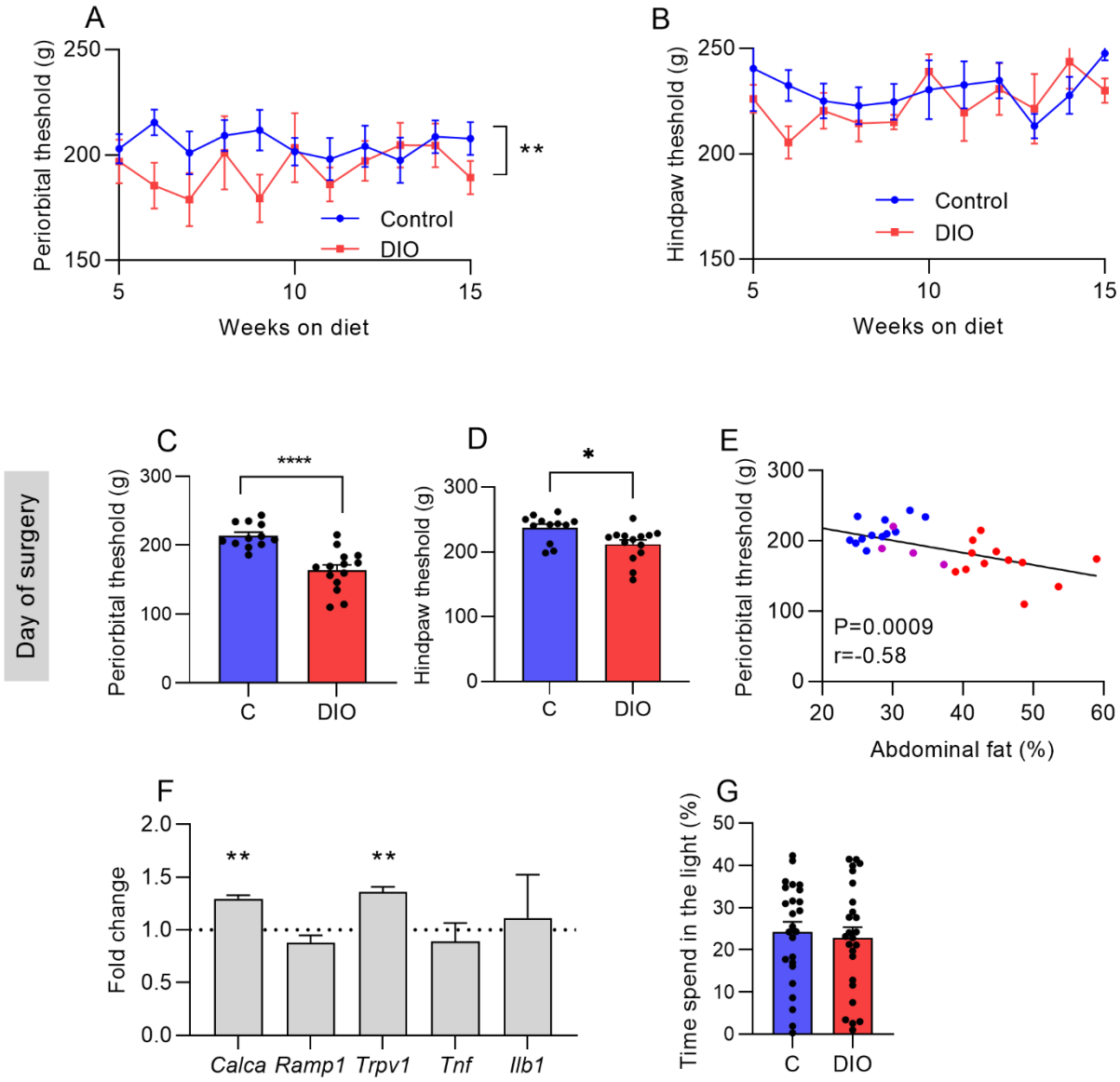

Figure 4. DIO induces cephalic allodynia: Peripheral and cephalic pain thresholds in female Sprague-Dawley rats on control and DIO rats. Longitudinal periorbital (**A**) and hindpaw (**B**) Von frey thresholds during obesogenisis. Periorbital (**C**) and hindpaw (**D**) Von frey testing on day 0. (**E**) Scatter graph of abdominal fat vs periorbital threshold on day 0, blue dots represent controls, red dots represent HFD rats. (**F**) Fold change in expression of *Calca*, *Ramp1*, *Trpv1*, *Tnf* and *Ilb1* in trigeminal ganglia of DIO rats, dotted line represents controls. (**G**) Photophobia testing of rats two weeks prior to surgery. Two-way repeated measure ANOVA for A and B. Unpaired students T-test for C and D. Pearson's correlation for E. *=P<0.05, **P<0.01 and ****=P<0.0001. Control N=12 and DIO= 14. Data presented as mean±SEM.

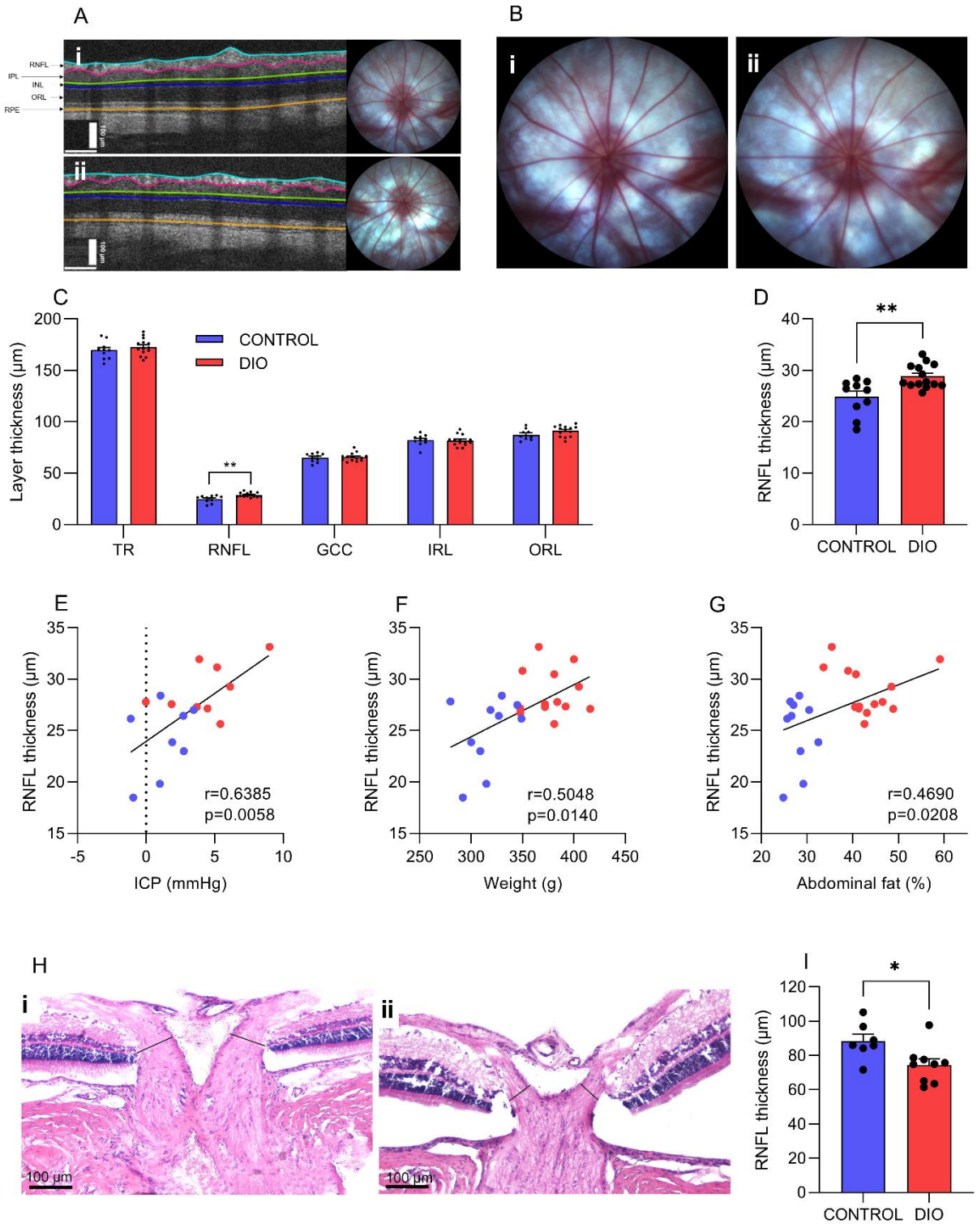

Figure 5. DIO and non-traumatic increased ICP alters neuroretinal structures: (**A**) Horizontally aligned OCT B-scans covering the peripapillary part circumferentially to the optic disc with manually adjusted segmentation lines. The DIO animal (**i**) is showing increased RNFL compared to a control animal (**ii**). RNFL= retinal nerve fiber layer, IPL=inner plexiform layer, INL=inner nucleus layer, ORL=outer retinal layers (including outer plexiform layer, outer nucleus layer, inner segments and outer segments) and RPE=retinal pigment epithelium. Scalebars equals 100 microns on the B-scan. (**B**) ODP with the optic nerve head (ONH) centered and focused in DIO (**i**) and a control (**ii**). (**C**) Graph presenting mean thickness in selected retinal layers. (**D**) RNFL thickness. (**E**) Scatter graph showing a positive association between RNFL thickness and mean ICP on day 3, where ICP has restored after craniotomy and postoperative medications were withdrawn. (**F-G**) Scatter graphs showing positive associations between RNFL thickness and weight (**F)**, and between RNFL and abdominal fat-% (**G**). (**H**) H&E micrographs of retinae, easure points (black solid lines) for RNFB thickness in the prelaminar region of the ONH in a control eye (**i**) and DIO eye (**ii**) Scale bar= 100µM. (**I**) RNFL thickness as assessed via the RNFB. Data in C, D and I are presented as mean±SEM. Unpaired T-test for D and I *=P<0.05, **=P<0.01

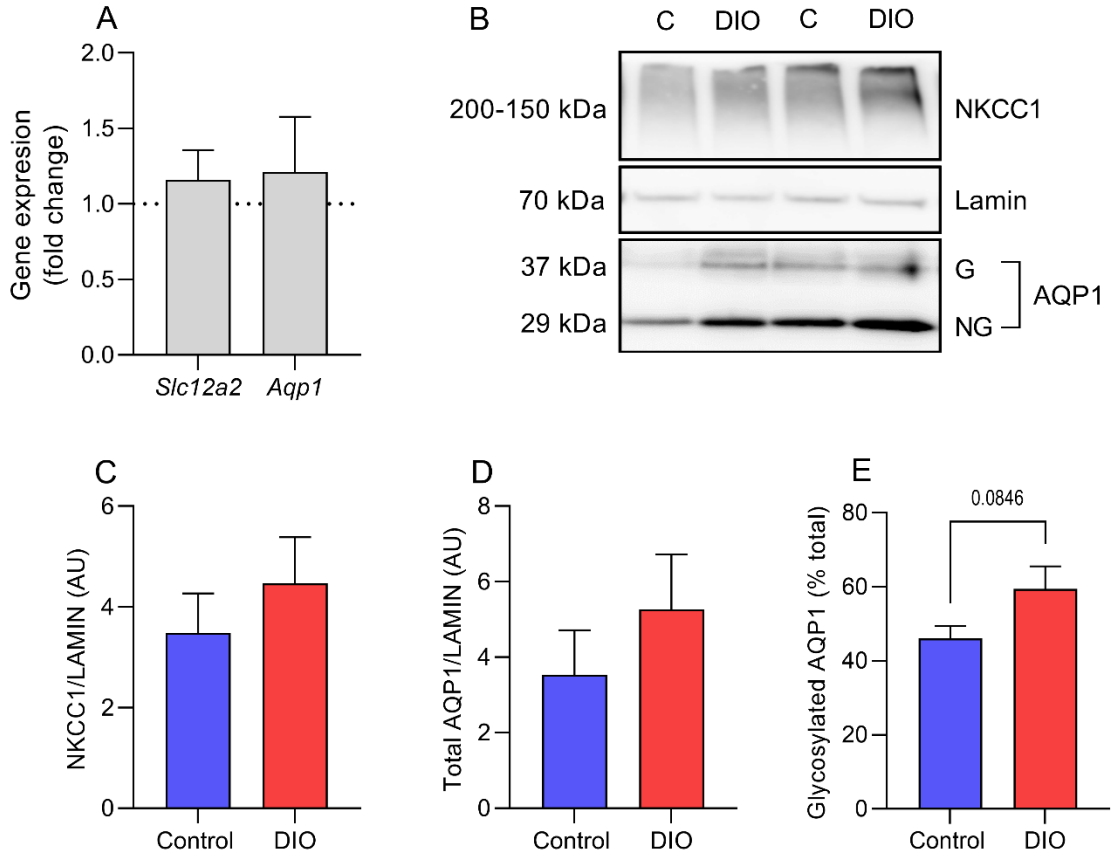

Figure 6. Expression of AQP1 and NKCC1 at CP: Expression of NKCC1 and AQP1 at CP in female Sprague-Dawley rats on control and HFD after 30 days implant with telemetric probes. Fold change of mRNA expression of NKCC1 and AQP1 in CP (A), and fold change of protein expression of NKCC1, total AQP1 and ratio between glycosylated AQP1 and total AQP1 (B) in CP. Dotted line represent mean for controls. Unpaired students t-test is done for A and B. Data are presented as mean±SEM.

Characteristics	Control	DIO
Headache related hypersensitivity		
Number (N)	12	14
Weight (g)	313.8±22.7	375.1±36.3****
Abdominal fat mass (g)	23.0±4.9	51.1±12.9****
Abdominal fat (%)	28.0±3.2	43.9±7.1****
Lean mass (g)	58.3±7.1	64.7±6.5*
OCT		
Number (N)	10	14
Weight (g)	316.6±22.2	370.8±35.5***
Abdominal fat mass (g)	22.8±3.8	49.4±11.0****
Abdominal fat (%)	27.9±2.34	43.2±6.2****
Lean mass (g)	58.5±7.6	65.2±7.2*
Intracranial pressure monitoring		
Number (N)	9	10
Weight (g)	316.0±17.3	365.9±37.8 **
Abdominal fat mass (g)	24.8±3.8	47.8±11.7****
Abdominal fat (%)	28.9±3.2	43.2±7.2****
Abdominal Lean mass (g)	60.3±4.5	63.3±6.6

Table 1. Characteristics of rats in each study: Weight, abdominal fat mass, abdominal fat % and lean mass in control and DIO rats in the headache, OCT and ICP studies. All tests are unpaired student's T-test. *=P<0.05, **=P<0.01, ***=P<0.001 and ****=P<0.0001). Data presented as mean±SD.

Table 2	**DIO**			**Control diet**		
OCT						
Number (N)		14			10	
Mean thickness, µm/microns	Both eyes	Right eye	Left eye	Both eyes	Right eye	Left eye
Total retinal (TR)	172.85±2.20	172.61±2.49	173.09±2.30	169.56±2.76	169.30±2.62	169.82±3.59
Retinal nerve fiber layer (RNFL)	28.82±0.61**	28.52±0.74	29.12±0.75	24.85±1.09	25.33±1.06	24.37±1.35
Ganglion Cell complex (GCC)	65.64±1.06	66.14±1.22	65.15±1.15	65.00±1.34	64.69±1.59	65.32±1.31
Inner retinal layers (IRL)	81.74±1.40	81.76±1.59	81.72±1.42	82.14±1.72	82.57±1.72	81.70±1.95
Outer retinal layers (ORL)	91.11±1.40	90.84±1.78	91.38±1.39	87.41±1.62	86.73±1.74	88.10±2.64
Histology						
Number (N)		9			7	
Mean thickness, µm/microns						
Retinal nerve fiber (RNF)		74.37±3.62*			88.36±3.97	

Table 2. OCT and histology data: There was no significant difference between right and left eye in any of the segmented layers of the peripapillary OCT scans in any of the groups. The mean RNFL from both eyes was significant thicker in the DIO animals. In the end of the study histology demonstrated

significant degeneration of the RNFB in the prelaminar region of the ONH in DIO animals compared to control animals. Data are presented as mean±SEM. *=P<0.05, **=P<0.01.

References

1. Olesen J, Gustavsson A, Svensson M, Wittchen H-U, Jönsson B. The economic cost of brain disorders in Europe. Eur J Neurol. 2012;19:155–62.

2. MacAulay N, Zeuthen T. Water transport between CNS compartments: Contributions of aquaporins and cotransporters. Neuroscience. Elsevier Inc.; 2010;168:941–56.

3. Berdahl JP, Fleischman D, Zaydlarova J, Stinnett S, Allingham RR, Fautsch MP. Body Mass Index Has a Linear Relationship with Cerebrospinal Fluid Pressure. Investig Opthalmology Vis Sci. 2012;53:1422.

4. Ren R, Wang N, Zhang X, Tian G, Jonas JB. Cerebrospinal fluid pressure correlated with body mass index. Graefe's Arch Clin Exp Ophthalmol. 2012;250:445–6.

5. Wakerley BR, Warner R, Cole M, Stone K, Foy C, Sittampalam M. Cerebrospinal fluid opening pressure: The effect of body mass index and body composition. Clin Neurol Neurosurg. Elsevier B.V.; 2020;188:105597.

6. Mollan SP, Aguiar M, Evison F, Frew E, Sinclair AJ. The expanding burden of Idiopathic Intracranial Hypertension. Eye. Nature Publishing Group; 2018;1.

7. Markey KA, Mollan SP, Jensen RH, Sinclair AJ. Understanding idiopathic intracranial hypertension: Mechanisms, management, and future directions. Lancet Neurol. 2016;15:78–91.

8. Yri HM, Fagerlund B, Forchhammer HB, Jensen RH. Cognitive function in idiopathic intracranial hypertension: A prospective case-control study. BMJ Open. British Medical Journal Publishing Group; 2014;4:e004376.

9. Rowe F, Sarkies N. The relationship between obesity and idiopathic intracranial hypertension. Int J Obes. 1999;23:54–9.

10. Szewka AJ, Bruce BB, Newman NJ, Biousse V. Idiopathic Intracranial Hypertension. J Neuro-Ophthalmology. 2013;33:4–8.

11. Uldall M, Bhatt DK, Kruuse C, Juhler M, Jansen-Olesen I, Jensen RH. Choroid plexus aquaporin 1 and intracranial pressure are increased in obese rats: Towards an idiopathic intracranial hypertension model? Int J Obes. Nature Publishing Group; 2017;41:1141–7.

12. Gerbaix M, Metz L, Ringot E, Courteix D. Visceral fat mass determination in rodent: validation of dual-energy x-ray absorptiometry and anthropometric techniques in fat and lean rats. Lipids Health Dis. 2010;9:140.

13. Eftekhari S, Westgate CSJ, Johansen KP, Bruun SR, Jensen RH. Long-term monitoring of intracranial pressure in freely-moving rats; impact of different physiological states. Fluids Barriers CNS. 2020;17:39.

14. Guild S-J, McBryde FD, Malpas SC. Recording of intracranial pressure in conscious rats via

telemetry. J Appl Physiol. 2015;119:576–81.

15. Munro G, Petersen S, Jansen-Olesen I, Olesen J. A unique inbred rat strain with sustained cephalic hypersensitivity as a model of chronic migraine-like pain. Sci Rep. Nature Publishing Group; 2018;8:1–13.

16. Christensen SL, Petersen S, Sørensen DB, Olesen J, Jansen-Olesen I. Cilostazol induces C-fos expression in the trigeminal nucleus caudalis and behavioural changes suggestive of headache with the migraine-like feature photophobia in female rats. Cephalalgia. SAGE Publications Ltd; 2018;38:452–65.

17. Christensen SLT, Petersen S, Sørensen DB, Olesen J, Jansen-Olesen I. Infusion of low dose glyceryl trinitrate has no consistent effect on burrowing behavior, running wheel activity and light sensitivity in female rats. J Pharmacol Toxicol Methods. Elsevier Inc.; 2016;80:43–50.

18. Andrews LE, Liu GT, Ko MW. Idiopathic Intracranial Hypertension and Obesity. Horm Res Paediatr. 2014;81:217–25.

19. Friesner D, Rosenman R, Lobb BM, Tanne E. Idiopathic intracranial hypertension in the USA: The role of obesity in establishing prevalence and healthcare costs. Obes Rev. Wiley/Blackwell (10.1111); 2011;12:e372–80.

20. Hornby C, Botfield HF, O'Reilly MW, Westgate C, Mitchell J, Mollan SP, et al. Evaluating the Fat Distribution in Idiopathic Intracranial Hypertension Using Dual-Energy X-ray Absorptiometry Scanning. Neuro-Ophthalmology. Taylor & Francis; 2018;42:99–104.

21. Alimajstorovic Z, Pascual-Baixauli E, Hawkes CA, Sharrack B, Loughlin AJ, Romero IA, et al. Cerebrospinal fluid dynamics modulation by diet and cytokines in rats. Fluids Barriers CNS. BioMed Central; 2020;17:10.

22. Martinez-Tejada I, Arum A, Wilhjelm JE, Juhler M, Andresen M. B waves: A systematic review of terminology, characteristics, and analysis methods. Fluids Barriers CNS. BioMed Central Ltd.; 2019. p. 1–15.

23. Bujalska IJ, Durrani OM, Abbott J, Onyimba CU, Khosla P, Moosavi AH, et al. Characterisation of 11β-hydroxysteroid dehydrogenase 1 in human orbital adipose tissue: A comparison with subcutaneous and omental fat. J Endocrinol. 2007;192:279–88.

24. Hoffmann J. Impaired cerebrospinal fluid pressure. 2018. p. 171–85.

25. Friedman DI, Quiros PA, Subramanian PS, Mejico LJ, Gao S, McDermott M, et al. Headache in Idiopathic Intracranial Hypertension: Findings From the Idiopathic Intracranial Hypertension Treatment Trial. Headache J Head Face Pain. 2017;57:1195–205.

26. Friedman DI, Rausch EA. Headache diagnoses in patients with treated idiopathic intracranial hypertension. Neurology. 2002;58:1551–3.

27. Yri HM, Rönnbäck C, Wegener M, Hamann S, Jensen RH. The course of headache in idiopathic

intracranial hypertension: A 12-month prospective follow-up study. Eur J Neurol. Wiley/Blackwell (10.1111); 2014;21:1458–64.

28. Mínguez-Olaondo A, Martínez-Valbuena I, Romero S, Frühbeck G, Luquin MR, Martínez-Vila E, et al. Excess abdominal fat is associated with cutaneous allodynia in individuals with migraine: A prospective cohort study. J Headache Pain. BioMed Central Ltd.; 2020;21:9.

29. Rossi HL, Broadhurst KA, Luu ASK, Lara O, Kothari SD, Mohapatra DP, et al. Abnormal trigeminal sensory processing in obese mice. Lippincott Williams and Wilkins; 2016;157:235–46.

30. Rossi HL, Luu AKSS, Devilbiss JL, Recober A. Obesity increases nociceptive activation of the trigeminal system. Eur J Pain (United Kingdom). Eur J Pain; 2013;17:649–53.

31. Peterlin BL, Rosso AL, Rapoport AM, Scher AI. Obesity and migraine: The effect of age, gender and adipose tissue distribution. Headache. 2010;50:52–62.

32. Charles A, Pozo-Rosich P. Targeting calcitonin gene-related peptide: a new era in migraine therapy. Lancet. 2019;394:1765–74.

33. Meents JE, Neeb L, Reuter U. TRPV1 in migraine pathophysiology. Trends Mol Med. 2010;16:153–9.

34. Laiginhas R, Guimarães M, Cardoso P, Santos-Sousa H, Preto J, Nora M, et al. Retinal Nerve Fiber Layer Thickness Decrease in Obesity as a Marker of Neurodegeneration. Obes Surg. 2019;29:2174–9.

35. Wang F, Lesser ER, Cutsforth-Gregory JK, Bhatti MT, Kilgore KP, Hodge DO, et al. Population-Based Evaluation of Lumbar Puncture Opening Pressures. Front Neurol. 2019;10.

36. Nusbaum DM, Wu SM, Frankfort BJ. Elevated intracranial pressure causes optic nerve and retinal ganglion cell degeneration in mice. Exp Eye Res. 2015;136:38–44.

37. Shen G, Link S, Kumar S, Nusbaum DM, Tse DY, Fu Y, et al. Characterization of Retinal Ganglion Cell and Optic Nerve Phenotypes Caused by Sustained Intracranial Pressure Elevation in Mice. Sci Rep. Nature Publishing Group; 2018;8:2856.